THE JOURNAL OF PHYSICAL CHEMISTRY C
A JOURNAL OF THE AMERICAN CHEMICAL SOCIETY

pubs.acs.org/JPCC

Article

Direct Experimental Determination of Ag Adatom Locations in TCNQ-Ag 2D Metal–Organic Framework on Ag(111)

Philip J. Mousley,* Luke A. Rochford, Hadeel Hussain, Stefania Moro, Pengcheng Ding, Gavin R. Bell, Giovanni Costantini, Christopher Nicklin, and D. Phil Woodruff*

Cite This: J. Phys. Chem. C 2023, 127, 4266–4272

Read Online

ACCESS | Metrics & More | Article Recommendations | Supporting Information

ABSTRACT: A previous investigation of the structure of TCNQ adsorbed on Ag(111) using normal-incidence X-ray standing waves (NIXSW) and density functional theory (DFT) provided indirect evidence that Ag adatoms must be incorporated into the molecular overlayer. New surface X-ray diffraction (SXRD) results, presented here, provide direct evidence for the presence and location of these Ag adatoms and clearly distinguishes between two alternative models of the adatom registry favored by two different DFT studies.

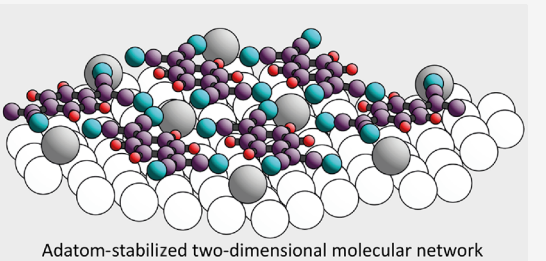

Adatom-stabilized two-dimensional molecular network

INTRODUCTION

Much of the motivation for investigating molecular adsorption on surfaces has been to understand the way the molecule–substrate interaction modifies the properties of the molecules, for example in lowering the energy barrier for intermolecular reactions to form the basis of heterogeneous catalysis. In addition, there are now many examples showing that a crystalline surface is not a simple rigid atomic-scale checkerboard but may also be modified structurally by the adsorption. One of the (relatively) more recently recognized manifestations of this effect is that deposition of some essentially planar molecules of potential relevance to molecular electronics onto metal surfaces can lead to the spontaneous incorporation of atoms from the underlying metal into the adsorbed molecular layer to produce a two-dimensional metal–organic framework (2D-MOF). In particular, evidence for the occurrence of this effect has been found for the prototypical electron acceptor molecule, (7,7,8,8-tetracyanoquinodimethane, TCNQ) and its fully fluorinated variant, F_4TCNQ, on some coinage metal (gold, silver, or copper) surfaces.[1−4]

Until relatively recently, there has been a dearth of quantitative experimental structural studies of these molecular adsorption systems, and the established wisdom concerning their structure was based only on the results of density functional theory (DFT) calculations. As a free molecule, the planar structure of TCNQ is very rigid due to the conjugated π-system that extends throughout the molecule, but when adsorbed on a metal surface, one or more electrons can be transferred to it. This leads the central quinoid ring to aromatize, which disrupts the π-conjugation,[5] while the peripheral carbon atoms become sp^3-hybridized (Figure 1a), causing the molecule to become far more flexible. Until recently, all DFT investigations of TCNQ and F_4TCNQ adsorbed on coinage metal surfaces have assumed no reconstruction of the metal surface and these calculations (performed without dispersion corrections) found a strong bending of the whole adsorbed molecule with the cyano N atoms lying up to 1.4 Å below the C atoms of the quinoid ring,

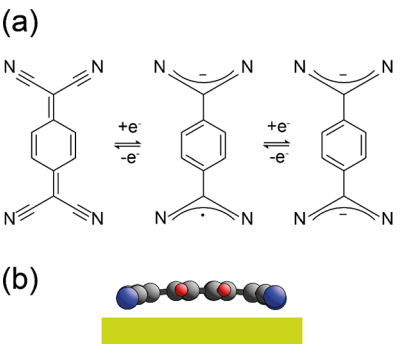

Figure 1. (a) Skeletal representation of TCNQ, $TCNQ^-$ and $TCNQ^{2-}$ showing the aromatization of the quinoid ring following electron take-up. (b) Typical side view of TCNQ adsorbed onto an unreconstructed coinage metal surface, according to DFT calculations. Atom coloring is H: red, C: black, and N: blue. The specific example shown is the result of dispersion-corrected DFT calculations for TCNQ adsorbed on Ag(100).[4]

Received: November 1, 2022
Revised: January 30, 2023
Published: February 15, 2023

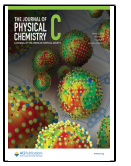

while the cyano C atoms lie midway between the N atoms and the quinoid ring[6−10] The molecule thus adopts an inverted bowl or umbrella conformation. Newer DFT calculations, which include dispersion corrections, show weaker bending but the same qualitative effect (e.g., see Figure 1b).[2,4]

A number of quantitative experimental structural studies using the normal-incidence X-ray standing wave (NIXSW)[11] technique have shown that this picture is not correct, at least for TCNQ adsorption on Ag(111)[2] and F_4TCNQ adsorption on Au(111)[3] and Ag(100).[4] By using core-level photoemission to monitor the X-ray absorption in the standing wavefield above the surface set up by a Bragg scattering condition from planes parallel to the surface, NIXSW provides a measure of the height of the chemically distinct atoms of the adsorbed molecule above the surface. For these adsorption systems, NIXSW results show that the N atoms in TCNQ or F_4TCNQ must occupy at least two different heights above the surface differing by several tenths of an ångström unit. Dispersion-corrected DFT calculations for these commensurate overlayer structures show that this result can only be reconciled with metal adatoms being incorporated into the molecular overlayer such that half the N atoms bond to metal adatoms while the other half of the atoms bond to underlying metal surface atoms. Unfortunately, while NIXSW measurements can distinguish the N atoms and chemically distinct C atoms in the adsorbed molecules, they cannot distinguish metal adatoms and substrate metal atoms; the associated chemical shift in the photoelectron binding energy is too small to detect. These experiments therefore provide only indirect evidence of metal adatom incorporation.

Indirect evidence of metal adatom incorporation is also provided by scanning tunneling microscopy (STM) images, most notably in the case of F_4TCNQ adsorbed on Au(111).[1] STM images are often regarded as a means of directly "seeing" surface atoms and molecules, but the interpretation of such images is not straightforward. Not all surface protrusions seen in constant-tunneling-current images correspond to the locations of surface atoms, and STM offers no way of distinguishing the elemental character of the atoms that do lead to such protrusions (e.g., ref 12). Simulated images based on the Tersoff−Hamman approach[13] are widely used to address this limitation, but this method takes no account of the crucial role of the electronic character of the imaging tip, so the results of such calculations may be indicative but are not definitive.

One method that offers a means to provide direct evidence for both the presence and locations of these metal adatoms is surface X-ray diffraction (SXRD). An important feature of X-ray diffraction is that the atomic scattering cross sections scale as the square of the atomic number, Z. As the constituent atoms of TCNQ and F_4TCNQ all have low values of Z ($\leq$9), while the adatoms of interest (Ag and Au) have very much higher atomic numbers (47 and 79), diffracted intensities from a molecular layer incorporating these metal adatoms are dominated by scattering from the adatoms. This effect is the basis of the "heavy atom" method used for solving the structures of complex macromolecules by X-ray diffraction.[14] We have recently shown[3] that SXRD provides clear direct evidence of Au adatom incorporation into an overlayer formed by deposition of F_4TCNQ on Au(111), also determining the lateral location and layer spacing of the adatoms, which are consistent with the results of dispersion-inclusive DFT calculations. Of course, the particularly high atomic number of Au is an especially favorable case to demonstrate the utility of the method. Here, we present the results of a similar study of the commensurate adsorption phase of TCNQ on Ag(111),[2] which also provides clear direct evidence for the presence and location of incorporated Ag adatoms. We also show that we can clearly distinguish between two alternative models of the adatom-surface lateral registry that were predicted by different published DFT calculations.[2,15]

METHODS

SXRD measurements were made using the UHV surface science end-station of beamline I07 of the Diamond Light Source.[16] The Ag(111) sample was first cleaned using cycles of argon ion bombardment and annealing. The $\begin{pmatrix} 2 & 5 \\ -8 & -2 \end{pmatrix}$ TCNQ commensurate adsorption phase was formed by in situ TCNQ deposition and annealing as described in detail previously.[2] Formation of this phase was confirmed by in situ LEED (low-energy electron diffraction) measurements. SXRD measurements used an incident photon energy of 21 keV and a grazing incidence angle of 0.3°.

RESULTS AND DISCUSSION

As in conventional X-ray diffraction determination of the structure of 3D-periodic crystal structures, SXRD involves the measurement and interpretation of diffracted beam intensities. However, while in XRD of 3D-periodic crystals, these measurements are of discrete *hkl* diffracted beams; the loss of periodicity perpendicular to the surface in SXRD means that diffracted beams are defined by discrete values of h and k, but l is a continuous variable. Measurements of the intensity of diffracted beams as a function of l are known as "rod scans", the reciprocal lattice points being replaced by reciprocal lattice "rods" perpendicular to the surface. Using the *hk* labels defined by the periodicity of the substrate, l scans of the intensity of beams with integral order values of h and k are known as crystal truncation rod (CTR) "rod scans". The "extra" diffracted beams due to the larger unit mesh of the surface structure are labeled with fractional order indices (following the standard convention of quantitative LEED structural studies), and the intensities of these beams are measured by fractional-order rod (FOR) scans.

Because the commensurate Ag(111)-TCNQ $\begin{pmatrix} 2 & 5 \\ -8 & -2 \end{pmatrix}$ mesh has only p2 symmetry whereas the Ag(111) surface has p3m symmetry, the diffraction pattern of this surface comprises an incoherent sum of the diffraction patterns of six symmetry-related domains. SXRD measurements were recorded from one of these domains, labeled as $\begin{pmatrix} 8 & 2 \\ 2 & 5 \end{pmatrix}$ (see Figure 2). The rod scan dataset collected from this domain comprised 10 CTR scans and 20 FOR scans. In addition, an "in-plane" dataset of the intensities of 38 fractional order diffracted beams was measured at a low value (0.4) of l. Figure S1 in the Supplementary Information identifies the diffracted beams measured in this investigation.

A standard problem of all XRD structural studies is that experiments measure diffracted beam intensities (the square modulus of the amplitudes) but not the amplitudes; as a result, the phase information is lost. This well-known "phase problem" means one cannot directly obtain the real-space structure from a Fourier transform of the measured dataset. However, a Fourier transform of the measured intensities, a

https://doi.org/10.1021/acs.jpcc.2c07683
J. Phys. Chem. C 2023, 127, 4266−4272

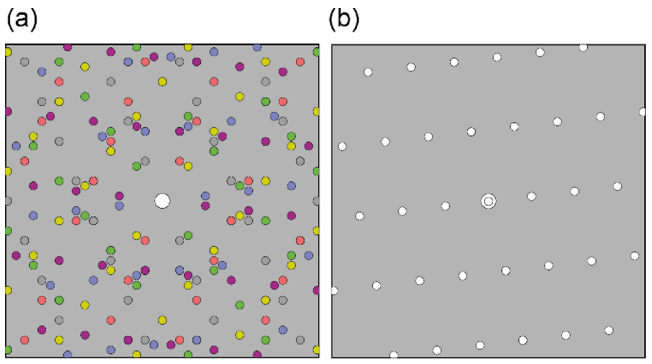

Figure 2. Simulations of the LEED pattern from the $\begin{pmatrix} 2 & 5 \\ -8 & -2 \end{pmatrix}$ commensurate phase of TCNQ adsorbed on Ag(111) using the LEEDpat program.[17] (a) Pattern expected from co-occupation of all six symmetry-related domains, the different colors identifying each domain. (b) Pattern from the single $\begin{pmatrix} 8 & 2 \\ 2 & 5 \end{pmatrix}$ domain from which all beam intensities were measured in this study.

Patterson function, provides a self-convolution (autocorrelation) of the real space structure, which can be helpful in guiding the subsequent full structure analysis. In the specific case of SXRD, a Fourier transform of "in-plane" intensities of fractional order beams provides a Patterson map that is a projection of all interatomic vectors onto the surface plane. In principle, this "in-plane" data set should correspond to intensities at values of $l = 0$, but in practice measurements, a low value of l must be used.

Figure 3a shows the Patterson map obtained from the experimental "in-plane" fractional order diffracted beam intensities. As all atoms in the surface structure are related to equivalent atoms in adjacent unit meshes by the primitive translation vectors of the unit mesh, the strongest features in the map simply define the corners of the unit mesh. Features within the unit mesh in the Patterson function correspond to interatomic vectors within the unit mesh, their relative intensities being determined by the atomic scattering cross sections of the component atoms together with the frequency of occupation of these vectors. If Ag adatoms are present within the unit mesh, the strongest features will be due to Ag−Ag vectors, the next strongest being Ag−N and Ag−C vectors, followed by C−C and C−N vectors. To interpret this experimental map, it is helpful to consider the likely structural models of this surface. The results of two detailed DFT calculations to identify the lowest energy structure have been published relatively recently,[2,15] and the corresponding structures are shown in Figure 4. Both calculations took account of the role of dispersion forces, but the earlier one[2] (hereafter referred to as DFT 2018) used the semi-empirical approach proposed by Grimme,[18] whereas the later calculation[15] (hereafter referred to as DFT 2020) used the more sophisticated Tkatchenko−Scheffler vdW^{surf} method (DFT + vdW^{surf}).[19] Both calculations showed that Ag adatom incorporation was energetically favored, but, as shown in Figure 4, the optimized structures differed in the lateral registry sites of the Ag adatoms relative to one another and to the underlying surface. In the DFT 2018 structure, the three Ag adatoms per unit surface mesh occupy bridging sites on a

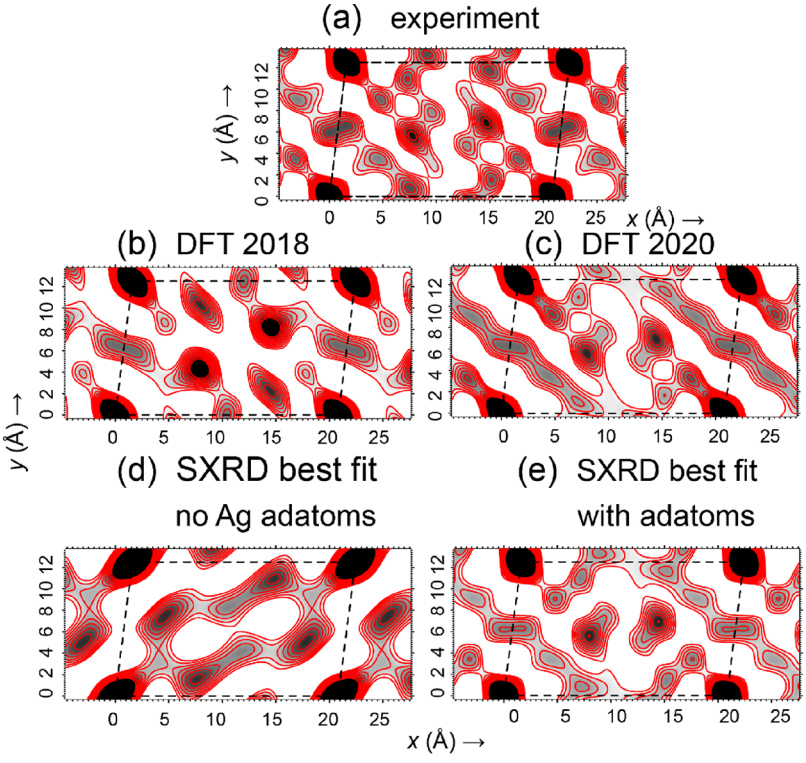

Figure 3. Patterson maps of experimental and simulated "in-plane" fractional order diffracted beam intensities; the dashed lines show the surface unit mesh. (a) Map obtained by Fourier transforming the experimental diffraction data. (b, c) Results of transforming a set of intensities calculated for the structural models deduced by the DFT calculations of refs 2 and 15, respectively. (d) Result of transforming calculated intensities based on the SXRD best fit model without Ag adatoms. (e) Result of transforming calculated intensities based on the best-fit structure including adatoms, as found in this SXRD full structure determination.

https://doi.org/10.1021/acs.jpcc.2c07683
J. Phys. Chem. C 2023, 127, 4266−4272

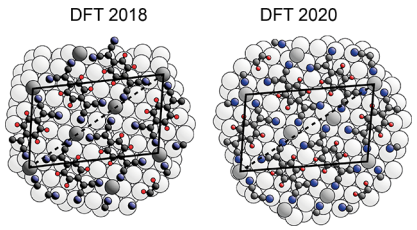

Figure 4. Plan views of the optimized structure of the Ag(111) $\begin{pmatrix} 8 & 2 \\ 2 & 5 \end{pmatrix}$-TCNQ surface phase according to the DFT calculations of refs 2 and 15. The Ag adatoms are shown with darker shading than the underlying Ag atoms of the bulk crystal. Other atoms are colored such that H: red, C: black, and N: blue. The dashed line superimposed along the diagonal of the unit mesh shows clearly that the adatoms are aligned along this diagonal in the DFT 2018 structure but not in the DFT 2020 structure.

periodic sub-mesh such that all nearest-neighbor adatom−adatom interatomic vectors are symmetrically equivalent, the adatom sites lying on the diagonal of the unit mesh, as shown by the dashed line superimposed on this structure in Figure 4. By contrast, in the DFT 2020 structure, the three Ag adatoms occupy different near-3-fold coordinated hollow sites, leading to several differently directed nearest-neighbor adatom−adatom interatomic vectors.

Patterson maps of diffracted intensities predicted for these two structures are shown in Figure 3b,c and reveal the impact of these different adatom registries. In particular, the fact that the Ag adatoms in the DFT 2018 model all lie along the diagonal of the unit mesh, with all adatom−adatom interatomic vectors being identical, leads to the two very strong peaks along the unit mesh diagonal. This effect is not seen in the experimental Patterson function. However, the dominant features of the predicted Patterson map for the DFT 2020 model are almost identical to those obtained from the experimental data. These Patterson maps therefore provide clear evidence for not only the presence of Ag adatoms in the TCNQ overlayer but also the fact that the relative lateral sites of these adatoms closely correspond to those of the DFT 2020 model and not the DFT 2018 model. Figure 3e shows the Patterson map obtained for simulated data from the surface structure (which includes Ag atoms; see below) that gives the best agreement with the complete experimental dataset. Further evidence for the presence of Ag adatoms is provided by Figure 3d, which shows the predicted Patterson map derived from the alternative model of the overlayer with no adatoms that was similarly optimized to give the best agreement with the experimental data. This simulated Patterson map is very different from the experimental one of Figure 3a.

In order to determine the surface structure in a more complete and quantitative fashion, it is necessary to use an indirect trial and error process in which the measured diffracted beam intensities are compared with those calculated for a sequence of alternative model structures. For this purpose, the ROD computer program[20] was used. In principle, this approach allows one to identify the best set of coordinates for all the atoms in the surface that have the lateral periodicity of the $\begin{pmatrix} 8 & 2 \\ 2 & 5 \end{pmatrix}$ unit mesh, which may include Ag atoms in the outermost layers of the crystal that are perturbed by the presence of the adsorbed layer. Notice that the fact that the integral order beams are common to the diffraction patterns of all six symmetry-related domains means that the CTR calculation must be performed for all six domains, the final results being incoherent summations of these six domain calculations. In fact, there is also overlap of some fractional order beams from different domains, so similar domain averages must be calculated for the relevant FORs and in-plane intensities.

In practice, the sensitivity of the technique to small changes in the exact relative positions of the weakly scattering C, N, and H atoms of the TCNQ molecules is very poor, as confirmed in exhaustive searches of these parameters in the earlier SXRD study of the Au(111)-F_4TCNQ surface.[3] The internal conformation of the TCNQ molecules was therefore fixed to be the same as in the DFT 2020 study. The structural search was then limited to the height and relative lateral positions of the TCNQ molecules and the Ag adatoms, together with the relaxation and rumpling amplitude of the outermost Ag(111) surface layer (a parameter identified as being important in the earlier SXRD study of the Au(111)-F_4TCNQ surface[3]). Included in these searches was the possibility that the overlayer contains no Ag adatoms (achieved by simply setting the occupancy of the adatoms to zero). The initial structural search started with the complete set of coordinates of the DFT 2020 structure (with appropriate scaling to account for the difference in the experimental and DFT lattice parameters). The parameters described were then allowed to vary, the ROD software[20] finding the best fit the complete dataset (CTRs, FORs, and in-plane intensities) using the normalized χ^2 value as the goodness-of-fit criterion.

The first important preliminary finding was that calculated diffracted intensities based on the "as-loaded" DFT 2020 structure showed poor agreement with the measured CTRs, with significant modulations not present in the experimental data. Figure 5a shows examples for a subset of four CTRs. This effect was finally found to be due to the small (∼2%) expansion of the outermost Ag layer spacing in this model as

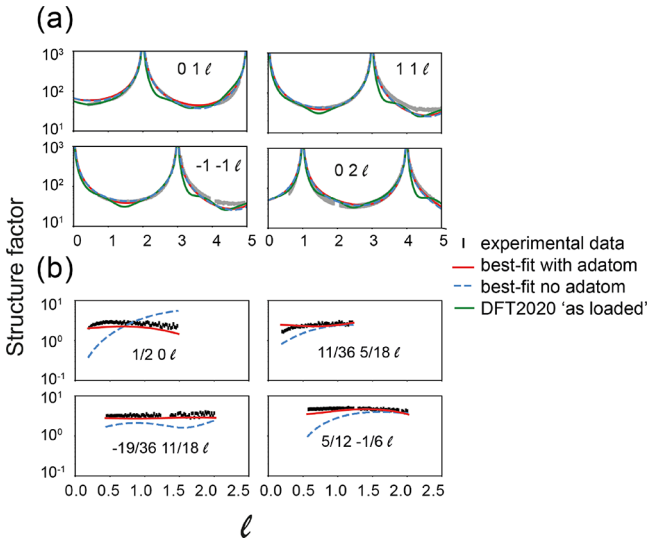

Figure 5. (a) Comparison of a subset of the experimentally measured CTRs (individual symmetric error bars) with simulations based on the "as-loaded" DFT 2020 structure (green line) and the best-fit structural model that includes adatoms (red line). (b) Comparison of a subset of the experimentally measured FORs (individual symmetric error bars) with simulations based on the best-fit structural models with (red) and without adatoms (dashed blue line).

https://doi.org/10.1021/acs.jpcc.2c07683
J. Phys. Chem. C 2023, 127, 4266−4272

well as the rumpling and small lateral displacements of the Ag atoms in the outermost layer. CTRs are extremely sensitive to these layer spacings of the high-density Ag layers. The DFT starting structure was therefore modified to have an ideal bulk termination of the Ag(111) substrate; hereafter, we refer to this as the "modified DFT structure". The subsequent structural optimization did then allow the possibility of rumpling perpendicular to the surface of the atoms in the outermost Ag layer as remarked above. Also shown in Figure 5a are the results of simulations based on the best-fit structural model with Ag adatoms, following the structural optimization described below.

Allowing complete freedom in the lateral positions of adatoms and molecules did lead to optimized structures with marginally lower χ^2 values, but the resulting structures had physically unrealistic interatomic distances. This can be attributed to the poor sensitivity to the exact location of individual molecules (comprising only weakly scattering atoms). This problem was also encountered in our earlier study of the Au(111)-F_4TCNQ system, but the problem is exacerbated in the Ag(111)-TCNQ system; in Au(111)-F_4TCNQ, the surface unit mesh contains only one Au adatom and one F_4TCNQ molecule, whereas in Ag(111)-TCNQ, there are three Ag adatoms and three TCNQ molecules in locally distinct sites within each surface unit mesh, leading to a larger number of structural parameters to be optimized simultaneously. Checks on the relative lateral positions of the overlayer components therefore focused on separate optimizations starting from the modified DFT 2020 model and from a similarly modified DFT 2018 model.

The best-fit structure (including Ag adatoms) found was that obtained by starting from the modified DFT 2020 model; this gave a χ^2 value of 2.47. For comparison, the optimized structure starting from the DFT 2018 model gave a χ^2 value of 3.75, while the best-fit no-adatom model starting from the modified DFT 2020 model gave a χ^2 value of 4.62. These values clearly indicate that the no-adatom model does not give a good description of the SXRD data and that an optimized structure based on the lateral positions of the DFT 2020 structure gives a better fit to the SXRD measurements than the optimized structure based on the lateral registry of the DFT 2018 structure.

These conclusions are fully consistent with those obtained by the more qualitative analysis of the Patterson maps of Figure 4 and are clearly supported by the comparisons of the experimental data with simulated data for the alternative model structures. A comparison for the in-plane data is shown in Figure 6 for the best-fit structures with and without adatoms, while similar comparisons for a subset of the FORs are shown in Figure 5b. The model structure including Ag adatoms clearly gives a better fit to the experimental data. By comparison, the CTRs are rather insensitive to this aspect of the structure; the complete set of measured CTRs are compared with the predictions of the "as-loaded" DFT 2020 structure and for the optimized "with adatoms" structure in Figure S2. The calculated CTRs for the no-adatom model are almost exactly coincident with those for the "with adatoms" model. As may be expected, the FORs are much more sensitive to this aspect of the structure. The complete set of experimental FORs are shown in Figure S3, compared with the simulations for the best-fit structures with and without Ag adatoms. While the simulations of the two alternative structures for some FORs show no strong preference for one

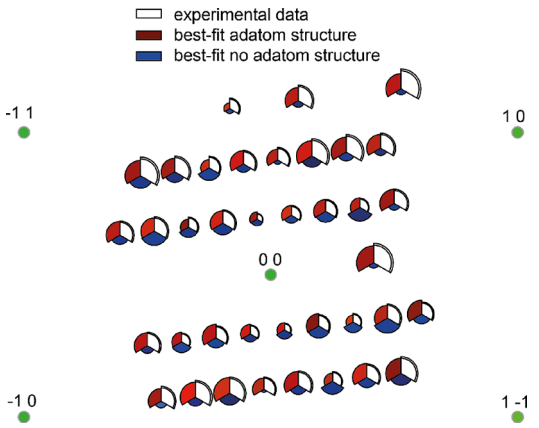

Figure 6. Comparison of the experimental and predicted in-plane structure factors of the full set of fractional order beams for the optimized SXRD structure shown in Figure S4. The locations of integral order beams are shown as green circles for reference. The areas of the one-third circular sections are proportional to the measured and calculated structure factors. Error estimates for the experimental data (white sections) are shown by inner and outer edges.

structure or the other, a significant number of the FORs show much better agreement with the with-adatom model.

In Table 1, key structural parameter values of the "as-loaded" DFT 2020 structure are compared with those of the best-fit SXRD structural model. There are small but marginally significant differences in the heights of the three TCNQ molecules and the three Ag adatoms per unit mesh, but what is more significant is the difference in the rumpling of the outermost Ag(111) layer. In particular, the amplitude of this rumpling in the SXRD structure is a factor of 2 larger than that found in the DFT calculations. This enhanced surface layer rumpling was also found in the SXRD investigation of the Au(111)-F_4TCNQ phase.[3] The origin of this effect is unclear. Of course, the DFT calculations simulate the bulk crystal and its surface by a very thin slab of metal atoms, so this could lead to a quantitative discrepancy in this parameter, but it seems unlikely that this would account for a discrepancy of a factor of 2. We also note that DFT calculations represent the 0 K structure and take no account of possible anharmonicity at higher temperatures. We have been unable to identify any alternative feature of the SXRD analysis that could account for this effect, so we conclude that a larger amplitude outer layer rumpling is indeed a necessary parameter of the interfacial model.

CONCLUSIONS

In summary, in agreement with previous indirect evidence from a combined NIXSW/DFT investigation,[7] our SXRD structure determination of the Ag(111)$\begin{pmatrix} 8 & 2 \\ 2 & 5 \end{pmatrix}$-TCNQ surface phase provides direct evidence of incorporation of Ag adatoms to form a 2D-MOF. We also show the relative lateral registry of the Ag adatoms, which is consistent with the results of the later DFT 2020 investigation rather than that of the original DFT 2018 study. More generally, our results for this Ag(111)-TCNQ surface reinforce the conclusions of our earlier study of the Au(111)-F_4TCNQ surface, namely, that SXRD offers a means to demonstrate directly the incorporations of metal adatoms into certain molecular adsorption phases. Of course, insofar as the method exploits the high atomic numbers of the

https://doi.org/10.1021/acs.jpcc.2c07683
J. Phys. Chem. C 2023, 127, 4266−4272

Table 1. Comparison of the Main Structural Parameter Values of the DFT 2020 Model and the Best-Fit SXRD Structure[a]

model	rumpling amplitude of top layer (Å)	rumpling amplitude of second layer (Å)	average molecule height−top layer height(Å)	average adatom height−top layer height(Å)	height range of molecules (Å)	height range of adatoms (Å)
DFT 2020	0.20	0.11	2.89	2.41	0.035	0.033
SXRD	0.40 ± 0.10	0.0 (fixed)	3.06 ± 0.01	2.56 ± 0.01	0.07 ± 0.01	0.033 (fixed)

[a]The internal conformation of the TCNQ molecules was fixed to that from the DFT 2020 study, and the height of each molecule is the mean height of the six carbon atoms of the quinoid ring.

"heavy" adatoms, the first example of Au adatoms was an especially favorable test case. Here, we show that Ag atoms are also sufficiently "heavy" for successful application of the method.

■ ASSOCIATED CONTENT

Supporting Information

The Supporting Information is available free of charge at https://pubs.acs.org/doi/10.1021/acs.jpcc.2c07683.

Further details of the SXRD experiments and full sets of theory/experiment comparisons of rod scan data; plan view of the best-fit structure (PDF)

Full set of atomic coordinates of the best-fit structure (XYZ)

■ AUTHOR INFORMATION

Corresponding Authors

Philip J. Mousley − *Diamond Light Source, Harwell Science and Innovation Campus, Didcot OX11 0DE, UK;* orcid.org/0000-0002-3666-3768; Email: philip.mousley@diamond.ac.uk

D. Phil Woodruff − *Department of Physics, University of Warwick, Coventry CV4 7AL, UK;* orcid.org/0000-0001-8541-9721; Email: d.p.woodruff@warwick.ac.uk

Authors

Luke A. Rochford − *School of Chemistry, University of Birmingham, Edgbaston, Birmingham B15 2TT, UK*

Hadeel Hussain − *Diamond Light Source, Harwell Science and Innovation Campus, Didcot OX11 0DE, UK;* orcid.org/0000-0002-1322-261X

Stefania Moro − *Department of Chemistry, University of Warwick, Coventry CV4 7AL, UK*

Pengcheng Ding − *Department of Physics, University of Warwick, Coventry CV4 7AL, UK*

Gavin R. Bell − *Department of Physics, University of Warwick, Coventry CV4 7AL, UK;* orcid.org/0000-0002-6687-7660

Giovanni Costantini − *School of Chemistry, University of Birmingham, Edgbaston, Birmingham B15 2TT, UK; Department of Chemistry, University of Warwick, Coventry CV4 7AL, UK;* orcid.org/0000-0001-7916-3440

Christopher Nicklin − *Diamond Light Source, Harwell Science and Innovation Campus, Didcot OX11 0DE, UK*

Complete contact information is available at: https://pubs.acs.org/10.1021/acs.jpcc.2c07683

Notes

The authors declare no competing financial interest.

■ ACKNOWLEDGMENTS

The authors thank the Diamond Light Source for allocations SI19105 and SI24284-1 at beamline I07 that contributed to the results presented here. S.M. acknowledges funding through a Chancellor's Scholarship by the University of Warwick.

■ REFERENCES

(1) Faraggi, M. N.; Jiang, N.; Gonzalez-Lakunza, N.; Langner, A.; Stepanow, S.; Kern, K.; Arnau, A. Bonding and Charge Transfer in Metal−Organic Coordination Networks on Au(111) with Strong Acceptor Molecules. *J. Phys. Chem. C* **2012**, *116*, 24558−24565.

(2) Blowey, P. J.; Velari, S.; Rochford, L. A.; Duncan, D. A.; Warr, D. A.; Lee, T.-L.; De Vita, A.; Costantini, G.; Woodruff, D. P. Re-evaluating How Charge Transfer Modifies the Conformation of Adsorbed Molecules. *Nanoscale* **2018**, *10*, 14984−14992.

(3) Mousley, P. J.; Rochford, L. A.; Ryan, P. T. P.; Blowey, P.; Lawrence, J.; Duncan, D. A.; Hussain, H.; Sohail, B.; Lee, T.-L.; Bell, G. R.; Costantini, G.; Maurer, R. J.; Nicklin, C.; Woodruff, D. P. Direct Experimental Evidence for Substrate Adatom Incorporation into a Molecular Overlayer. *J. Phys. Chem. C* **2022**, *126*, 7346−7355.

(4) Ryan, P.; Blowey, P. J.; Sohail, B. S.; Rochford, L. A.; Duncan, D. A.; Lee, T.-L.; Starrs, P.; Costantini, G.; Maurer, R. J.; Woodruff, D. P. Thermodynamic Driving Forces for Substrate Atom Extraction by Adsorption of Strong Electron Acceptor Molecules. *J. Phys. Chem. C* **2022**, *126*, 6082−6090.

(5) Milián, B.; Pou-Amérigo, R.; Viruela, R.; Ortí, E. A Theoretical Study of Neutral and Reduced Tetracyano-p-Quinodimethane (TCNQ). *J. Mol. Struct.: THEOCHEM* **2004**, *709*, 97−102.

(6) Stradi, D.; Borca, B.; Barja, S.; Garnica, M.; Díaz, C.; Rodríguez-García, J. M.; Alcami, M.; de Parga, A. L. V.; Miranda, R.; Martín, F. Understanding the Self-Assembly of TCNQ on Cu(111): a Combined Study Based on Scanning Tunnelling Microscopy Experiments and Density Functional Theory Simulations. *RSC Adv.* **2016**, *6*, 15071−15079.

(7) Romaner, L.; Heimel, G.; Brédas, J.-L.; Gerlach, A.; Schreiber, F.; Johnson, R. L.; Zegenhagen, J.; Duhm, S.; Koch, N.; Zojer, E. Impact of Bidirectional Charge Transfer and Molecular Distortions on the Electronic Structure of a Metal-Organic Interface *Phys. Rev. Lett.* **2007**, *99*, No. 256801.

(8) Tseng, T.-C.; Urban, C.; Wang, Y.; Otero, R.; Tait, S. L.; Alcamí, M.; Écija, D.; Trelka, M.; Gallego, J. M.; Lin, N.; et al. Charge-Transfer-Induced Structural Rearrangements at Both Sides of Organic/Metal Interfaces. *Nat. Chem.* **2010**, *2*, 374−379.

(9) Barja, S.; Stradi, D.; Borca, B.; Garnica, M.; Díaz, C.; Rodriguez-García, J. M.; Alcamí, M.; de Parga, A. L. V.; Martín, F.; Miranda, R. Ordered Arrays of Metal−Organic Magnets at Surfaces. *J. Phys.: Condens. Matter* **2013**, *25*, No. 484007.

(10) Martínez, J. I.; Abad, E.; Flores, F.; Ortega, J. Simulating the Organic-Molecule/Metal Interface TCNQ/Au(111). *Phys. Status Solidi B* **2011**, *248*, 2044−2049.

(11) Woodruff, D. P. Surface Structure Determination Using X-ray Standing Waves. *Rep. Prog. Phys.* **2005**, *68*, 743−798.

(12) Woodruff, D. P. Is Seeing Believing? Atomic-Scale Imaging of Surface Structures Using Scanning Tunnelling Microscopy. *Curr. Opin. Solid State Mater. Sci.* **2003**, *7*, 75−81.

(13) Tersoff, J.; Hamann, D. R. Theory of the Scanning Tunneling Microscope. *Phys. Rev. B* **1985**, *31*, 805−813.

(14) Drenth, J., *Principles of Protein X-ray Crystallography*; Springer Science, 2007.

(15) Blowey, P. J.; Sohail, B.; Rochford, L. A.; Lafosse, T.; Duncan, D. A.; Ryan, P. T. P.; Warr, D. A.; Lee, T.-L.; Costantini, G.; Maurer,

R. J.; Woodruff, D. P. Alkali Doping Leads to Salt Formation in a Two-Dimensional Metal-Organic Framework. *ACS Nano* **2020**, *14*, 7475−7483.
(16) Nicklin, C.; Arnold, T.; Rawle, J.; Warne, A. Diamond Beamline I07: a Beamline for Surface and Interface Diffraction. *J. Synchrotron Radiat.* **2016**, *23*, 1245−1253.
(17) *LEEDpat4: LEED pattern analyser Home page*. https://www.fhi.mpg.de/958975/LEEDpat4 (accessed 2023-01-27)
(18) Grimme, S. Semiempirical GGA-Type Density Functional Constructed with a Long-Range Dispersion Correction. *J. Comput. Chem.* **2006**, *27*, 1787.
(19) Ruiz, V. G.; Liu, W.; Zojer, E.; Scheffler, M.; Tkatchenko, A. Density-Functional Theory with Screened van der Waals Interactions for the Modelling of Hybrid Inorganic-Organic Systems. *Phys. Rev. Lett.* **2012**, *108*, No. 146103.
(20) Vlieg, E. ROD: a Program for Surface X-Ray Crystallography. *J. Appl. Crystallogr.* **2000**, *33*, 401.

https://doi.org/10.1021/acs.jpcc.2c07683
J. Phys. Chem. C 2023, 127, 4266−4272